Available online at www.sciencedirect.com
SCIENCE DIRECT®
Polymer 44 (2003) 7709–7719
polymer
www.elsevier.com/locate/polymer

Syntheses and characterizations of in situ blended metallocence polyethylene/clay nanocomposites

Shiao-Wei Kuo[a], Wu-Jang Huang[b], Si-Bo Huang[a], Hsin-Ching Kao[a], Feng-Chih Chang[a,*]

[a]*Institute of Applied Chemistry, National Chiao Tung University, Hsin Chu 30050, Taiwan, ROC*
[b]*Department of Environmental Science and Engineering, National Ping-Tung University of Science and Technology, Ping-Tun, Taiwan, ROC*

Received 25 July 2003; received in revised form 29 August 2003; accepted 7 October 2003

Abstract

In this paper, we report the preparation of in situ blends of metallocence polyethylene (mPE) with montmorillonite (clay). The polymerization activity of polyethylene decreases upon increasing the amount of the clay feed. The mPE nanocomposites still possess their original melting and crystallization temperatures, but the melting and crystallization enthalpies decrease upon increasing the clay content. In addition, the polymer interaction parameter between mPE and exfoliated clay sheets was calculated to be −0.204 based on a modified Kim–Bae equilibrium melting depression equation. All of the isothermal crystallization kinetics data fit well to the Avrami crystallization equation. We found that increasing the clay content results in a faster rate of crystallization, but pure mPE still crystallizes the fastest. Using a small amount of pretreated clay results in a more homogeneous and finer dispersion of the clay in the polymer matrix, as determined by wide-angle X-ray diffraction and transmission electron microscopy analyses. Both the values of $T_{1\rho}^{H}$ in the solid-state NMR spectra of the fast and slow components show increment upon increasing the clay content, which indicates that either the mobile phase tends to increase its rigidity in the clay-containing system.

Keywords: Metallocence polyethylene; Clay; Nanocomposites

1. Introduction

Clay reinforced polymer nanocomposites possess high flame resistance, high glass transition temperatures, high decomposition temperatures, high impact strengths, high barrier properties and high crystallization rates [1–4], and have potential applications as functional fibers and in the engineering of plastics. Traditionally, the clay is melt-blended with polyolefins, such as polyethylene (PE) and polypropylene (PP) [5]. Polyolefins are usually produced from metal-coordination polymerization using the heterogeneous Ziegler-Natta catalyst. Recently, new developments in homogeneous Zigler-Natta type catalysts (metallocence catalyst) have demonstrated that they are highly active in the polymerization of α-olefins [6–10]. The use of modified metallocence catalysts in PE polymerization has been reported often in the literature [11], but few reports have focused on preparing in situ formed nanocomposites [12,13].

In this study, we have prepared metallocence polyolefin nanocomposites using the so-called in situ blending method. Metallocence polyethylene (mPE) is blended with clay during the polymerization stage. The advantages of this method are (1) the one-pot synthesis of the metallocence polymer nanocomposites, (2) the improved compatibility of the clay and polymer matrix, and (3) the enhanced clay dispersity. The residual water present in the free space between clay layers, however, may de-active the metallocence catalyst, and so the reaction activity of mPE decreases with increasing the clay content. In this study, we attempted to improve the catalyst activity in mPE nanocomposite polymerization through sequential addition of clay, methylaluminoxane (MAO), metallocence catalyst, and the ethylene monomer, as well as by changing the reaction temperature and the quantity of MAO. We have used solid-state NMR spectroscopic $T_{1\rho}^{H}$ measurements to calculate the relative fractions of crystalline and mobile phases of the

* Corresponding author. Tel.: +886-3-5727077; fax: +886-3-5719507.
E-mail address: muddaxac.ac87g@nctu.edu.tw (F.C. Chang).

0032-3861/$ - see front matter © 2003 Elsevier Ltd. All rights reserved.
doi:10.1016/j.polymer.2003.10.007

resultant mPE nanocomposites and to determine their relationship with the clay content.

It is well known that measuring polyethylene crystallization kinetics is difficult because of its fast rate [14–16]. The PE crystallization process is affected by such testing conditions as the crystallization temperature, the cooling rate and thermal gradients. Using thinner samples for DSC usually can minimize the effect of thermal gradients, but the transient response due to the instrument's design will always be present. The modified conventional isothermal and non-isothermal crystallization methods can be used to obtain fairly good estimates of crystallization rates. Crystallization at a relative lower temperature does not provide significant evidence for molecular segregation or reorganization and lower Avrami exponents are usually observed from the melt crystallization of PE [15].

Kim and Bae [17] have modified the Flory–Huggins melting point depression theory by incorporating the Debye–Huckel lattice concept induced by ion–ion interactions in the polymer electrolyte. The existence of electrolyte or charged species in a crystallizable polymer solution can result in coordination between the polymer and the salt and a depression in its equilibrium melting point as a result of the development of stable polymer crystals. In this paper we report that, interestingly, the mPE/clay nanocomposites show a behavior in the depression of their equilibrium melting temperatures that is similar to that of polymer/inorganic salt systems.

2. Experimental

2.1. Clay pretreatment

Montmorillonite (clay) was pretreated with cetyl pyridinium chloride (CPC) at a molar ratio of 1:1. The mixture was vigorously stirred in water for 18 h, and then filtered, washed, freeze-dried, and kept at 60 °C under vacuum for 12 h. The untreated clay was washed with water and dried at 120 °C under vacuum for 48 h.

2.2. Metallocence polyethylene polymerization routes

Ethylene was polymerized using the ansa-metallocence catalyst $Et(Indenyl)_2ZrCl_2$ and the MAO co-catalyst to prepare mPE. For all of the experiments, the polymerization temperature was set at room temperature (or 50 °C if required), the catalyst/co-catalyst ratio was between 2500 and 10,050, and the ethylene pressure was maintained at 19–21 psi. The total volume of the system was 60–65 ml and the polymerization time was 1 h. The amount of metallocence catalyst was ca 0.5 mg and acidic methanol (10 ml) was used to terminate the polymerization. An excess amount of acetone was added into the polymer solution and then it was dried for 8 h at 50 °C under vacuum.

The clay, metallocence catalyst, and a toluene solution of MAO were added sequentially through three different routes as outlined in Scheme 1. In Route 1, the surfactant-pretreated clay was mixed directly with the ethylene monomer, catalyst, and co-catalyst to begin the polymerization at room temperature. In Route 2, the surfactant-pretreated clay was mixed initially with the MAO co-catalyst at 30 °C for 1.5 h and then mixed with the metallocence catalyst at 55 °C for another 0.5 h; the catalyst/clay mixture was then mixed with ethylene monomer to begin the polymerization for 1 h under ambient conditions. In Route 3, the surfactant-pretreated clay was first mixed and agitated with MAO co-catalyst at 30 °C for 2.5 h, and then mixed with the metallocence catalyst at 55 °C for another 2 h; the catalyst/clay mixture was then mixed with ethylene to begin the polymerization for 1 h under ambient condition.

2.3. Characterization

A Perkin–Elmer DSC-7 instrument was used with heating and cooling rates of 10 °C/min, and a scanning range from 30 to 250 °C to determine the thermal transition temperatures. The DSC instrument was also employed in the isothermal crystallization study. A precipitated sample of ca 3–5 mg was first heated to 200 °C in an aluminum pan in the DSC furnace and maintained at that temperature for 10 min. This procedure was undertaken to ensure total relaxation of the sample and to eliminate the potential influence of thermal history. The sample was then cooled rapidly to the preset crystallization temperature to begin the isothermal crystallization. After crystallization was complete, the sample was re-heated at a rate of 10 °C/min to determine the melting temperature. Before discussing the crystallization data of the mPE homopolymer and its clay nanocomposites, we emphasize that the polymer sample was recovered by non-solvent precipitation and purification. We assume that the metallocence catalyst is washed out

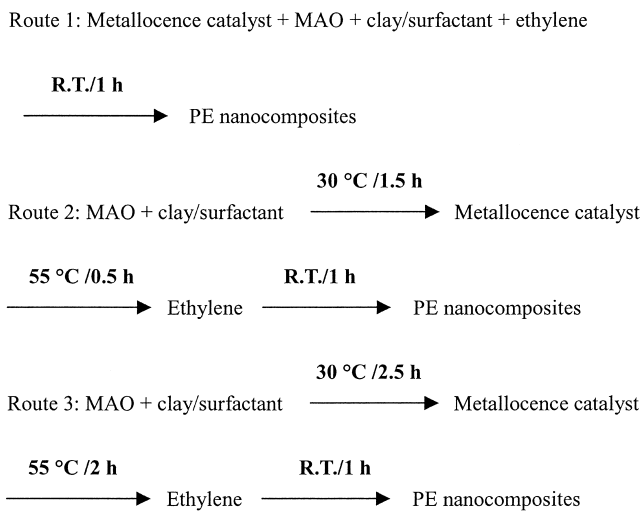

Scheme 1. Polymerization routes of polyethylene nanocomposites.

during this purification process and so it is not expected to affect the crystallization behavior. X-ray diffraction spectra were collected on an M18XHF-SRA instrument (MacScience Co., Japan) using Cu Kα radiation, and Bragg's law ($\lambda = 2d \sin\theta$) was used to compute the spacing. High-resolution solid-state ^{13}C NMR spectroscopy experiments were carried out at room temperature using a Bruker DSX-400 spectrometer operating at resonance frequencies of 399.53 and 100.47 MHz for ^{1}H and ^{13}C, respectively. The ^{13}C CP/MAS spectra were measured with a 3.9-μs 90° pulse, a 3 s pulse delay time, an acquisition time of 30 ms, and 2048 scans. All NMR spectra were taken at 300 K using broad-band proton decoupling and a normal cross-polarization pulse sequence. A magic angle sample-spinning (MAS) rate of 5.4 kHz was used to avoid absorption overlapping. The proton spin-lattice relaxation time in the rotating frame ($T_{1\rho}^{H}$) was determined indirectly by carbon nucleus observation using a 90°-τ-spin lock pulse sequence prior to cross polarization. The data acquisition was performed by ^{1}H decoupling with delay time (τ) ranging from 0.1 to 12 ms and a contact time of 1.0 ms. A micrograph of a microtomed section of the PE/clay hybrid of 60–100 nm thickness, mounted in epoxy resin, was conducted with a transmission electron microscope (JEM-2000FX, Joel Company, Japan) at an acceleration voltage of 100 kV.

3. Results and discussion

3.1. Effect of polymerization activity in Route 1

Table 1 summarizes the polymerization activity, the melting and crystallization temperatures, and the melting and crystallization enthalpies of the products formed using pure clay that had not been pretreated with surfactant. The polymerization activities of polyethylene decrease upon increasing the amount of clay feed. This observation may be due to the residual water remaining in the free space between the clay layers, which tends to de-activate the cationic center of the metallocence catalyst. From analysis of the DSC traces, we determined that these mPE nanocomposites have melting and crystallization temperatures close to those of pure mPE, but have substantially decreased crystallinity (in terms of melting and crystallization enthalpies) upon increasing the clay content. This result is consistent with others reported in the literature [18,19]. Wide-angle X-ray diffraction (WAXD) patterns show that these mPE nanocomposites still maintains the same orthorhombic crystallite form of pure mPE (Section 3.1.1). Table 1 also summarizes the corresponding data from the mPE formed using the surfactant-pretreated clay. Again, the polymerization activity of mPE decreases upon increasing the amount of the clay feed. From the DSC traces, we observe that these mPE nanocomposites all possess the same values of T_m and T_c as the original pure mPE.

3.1.1. WAXD and TEM of metallocence PE nanocomposites in Route 1

Fig. 1(a) and (b) shows the WAXD patterns of mPE nanocomposites obtained when the clay was pretreated with CPC; a new peak appears at $2\theta = 19.8$. A more homogeneous and finer dispersion of clay in the polymer matrix is obtained when the pretreated clay content is less than 10 wt% since no Bragg scattering was detected between 1 and 10° (2θ). Fig. 2 displays the TEM micrograph of a thin section of mPE nanocomposites having 2.4 wt% of clay; the dark lines denote the silicate layers. The surfactant, CPC, intercalates into the clay by attraction between its organic cation and the silicate surface, which renders the hydrophobic silicate surface organophilic, and the stacked layers are randomly distributed in the mPE matrix. This result indicates that the clay has been exfoliated with no regular repeated distance observed between the layers. When the polymer is formed with a pretreated clay content of greater than 10 wt%, a diffraction peak from the clay appears at 1–4°, which is an indication that this nanocomposite has intercalated clay clusters in the polymer matrix.

3.2. Effect of polymerization activity in Routes 2 and 3

3.2.1. Rate de-activation with and without pretreatment of clay

Water is known to cause catalyst de-activation in

Table 1
Polymerization condition and thermal properties of mPE/clay nanocomposites formed from with un-pretreated and pretreated clay

Clay content (wt%)	Activity (g polymer/mol × catalyst × hrs)	T_m (°C)	ΔH_m (J/g)	T_c (°C)	ΔH_c (J/g)
Un-pretreated Clay					
0	1.8×10^6	131.3	155.3	114.8	156.1
4.8	1.0×10^6	131.9	119.2	116.1	108.9
6.78	7.2×10^5	126.4	83.6	112.3	82.3
Pretreated Clay					
0	1.8×10^6	131.3	155.3	114.8	156.1
2.4	1.0×10^6	130.0	90.1	112.1	85.6
7.3	9.0×10^5	131.2	70.0	113.0	61.9
12.2	8.9×10^5	131.2	30.5	115.0	23.0

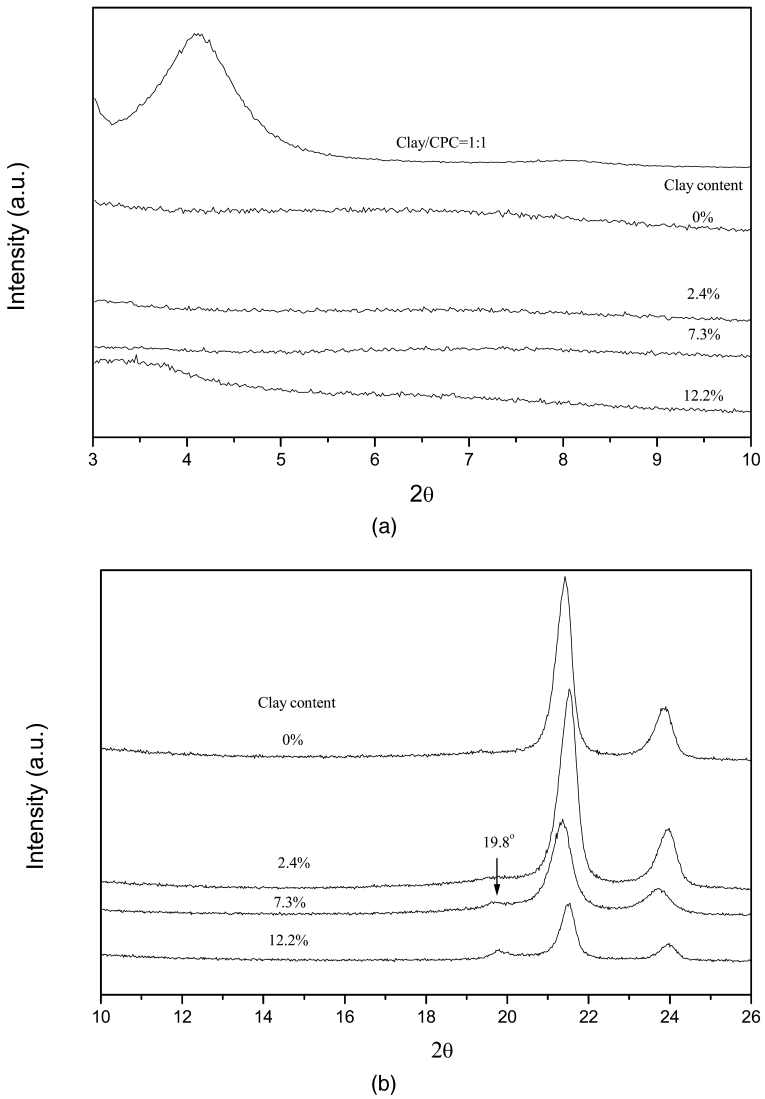

Fig. 1. WAXD pattern of metallocence PE nanocomposites using the pretreated clay of (a) $2\theta = 3-10°$ and (b) $2\theta = 10-26°$.

metallocence polymerization. Fig. 3 shows that the decrease in the rate of metallocence polymerization for the clay with CPC pretreatment is slower than that without pretreatment when the clay content is greater than 2.4 wt%. When the clay is pretreated with CPC, the residual water content in the clay becomes relatively low because of the hydrophobic nature of CPC, which thus deactivates the polymerization to a lesser degree.

Table 2 provides a comparison between the polymerization activity and clay content using the different polymerization Routes 1–3. For Route 1, the polymerization activity decreases upon increasing the clay feed content and reducing the amount of MAO. The residual water present in the free spaces between the clay's layers may deactivate of the cationic center of the metallocence catalyst.

Routes 2 and 3 provide a higher reactivity (ca two-fold) relative to that of Route 1 under similar reaction conditions (when 46 ml of MAO is used). A comparison of Routes 2 and 3 demonstrates that extending the time during which the surfactant/clay mixture is treated with MAO does not enhance the activity. The polymerization activity of Route 2 using 46 ml of MAO is close to that for Route 1 when using 80 ml of MAO. The activity increases by nearly one order of magnitude when the amount of MAO is increased from 23 to 80 ml. We conclude that the polymerization activity can be improved substantially through sequential addition of the clay, MAO, the metallocence catalyst, and the ethylene monomer, as well as by changes in the reaction temperature and the amount of MAO.

3.2.2. Wide-angle X-ray diffraction of metallocence PE nanocomposites formed by Route 2

Fig. 4(a) and (b) shows that a homogeneous and fine dispersion of clay is obtained in the polymer matrix when the clay/surfactant mixture and MAO are pretreated using Route 2. The corresponding WAXD pattern exhibits no Bragg scattering of the clay diffraction peak, which is similar to the situation observed in Fig. 1. This new peak

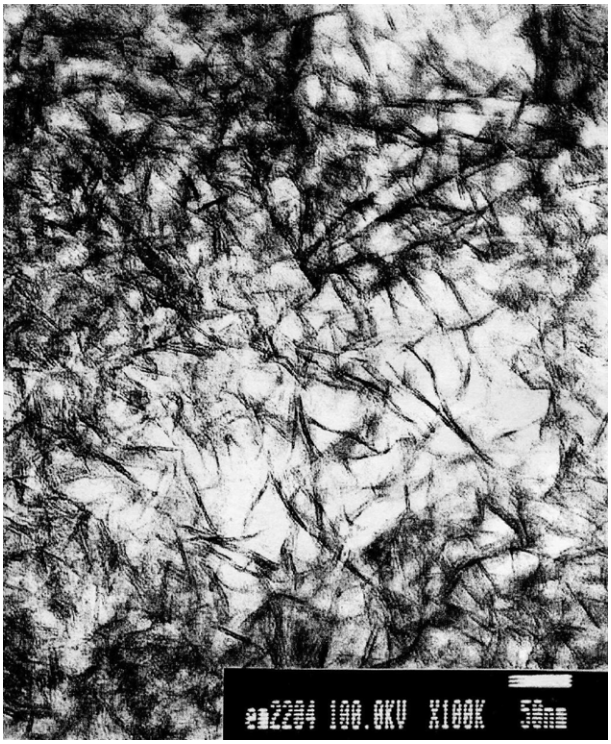

Fig. 2. TEM micrograph of a thin section of mPE nanocomposites formed using 2.4 wt% of clay.

presumably arises from the formation of a nematic phase, which we discuss below.

3.3. Solid state NMR characterization

Solid-state NMR spectroscopic $T_{1\rho}^{H}$ measurements have been used previously to determine the relative quantities of crystalline and amorphous phases in polymers [20–23]. Fig. 5 shows the $T_{1\rho}^{H}$ decay curves for mPE nanocomposites formed by Route 1 with varying clay content. Clearly, all of the decay data can be fitted by two exponential decay functions: a fast decay component for the mobile phase (amorphous phase) and a slow decay component for the rigid phase (crystalline phase). Fig. 6 shows the effect of the clay content on the fraction of these two components and their respective values of $T_{1\rho}^{H}$.

The fraction of the slow component decreases, and the fraction of the fast component increases, upon increasing the clay content. Their corresponding WAXD peaks, displayed in Fig. 1(b), clearly show that mPE crystallinity decreases with increasing clay content. We note with interest that both values of $T_{1\rho}^{H}$ from the fast and slow components show increment with increasing clay content. The fast-decay component tends to have a larger value of $T_{1\rho}^{H}$, which indicates that either the mobile phase tends to increase its rigidity or that a nematic phase is possibly formed in the clay-containing system, as has been suggested previously [17,24]. Therefore, the new diffraction peak may be a result of the nematic phase. The absence of any thermal transition of the new nematic phase observed in the DSC traces in PE nanocomposites due probably to a small melting enthalpy of the nematic phase.

3.4. Crystallization behaviors of mPE/clay nanocomposites

Fig. 7 displays isothermal crystallization data and the crystallinity of mPE homopolymer and nanocomposites as a function of time. All these data fit well to the Avrami crystal growth equation, as shown in Fig. 8. The fitted crystallization kinetic parameter k and n are summarized in Table 3. We observe retardation of crystallization resulting from the presence of the clay in all of the PE nanocomposites; the mPE homopolymer has a faster rate of crystallization than any of the mPE nanocomposites. We assume that the clay can be defected to induce the polymer melt nucleation process. The clay's retardation effect on the crystallization behavior is discussed in the following sections. Fig. 9 shows the half time for crystallization as a function of the

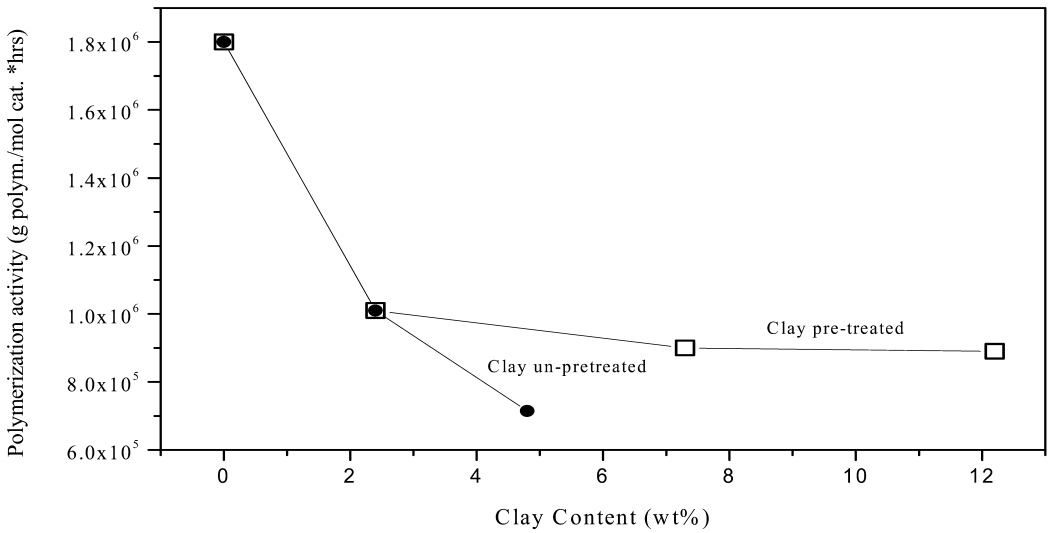

Fig. 3. Plots of the polymerization activity versus the clay feed.

Table 2
Effects of the clay feed treatment and other conditions on the polymerization activity

Route	MAO (ml)	Al/Zr (molar ratio)	Reaction time (min)	Clay content (wt%)	Activity (g/mol Zr × h)
Different Routes					
1	80	10,043	60	0	1.8×10^6
1	80	10,043	60	2.4	1.0×10^6
1	80	10,043	60	7.3	9.0×10^5
1	80	10,043	60	12.2	8.9×10^5
1	46	5775	60	16.5	3.8×10^5
2	46	5775	60	12.3	6.7×10^5
3	46	5775	60	12.8	5.7×10^5
Different reaction time					
2	46	5775	10	15.7	3.2×10^6
2	46	5775	30	13.7	1.2×10^6
2	46	5775	60	12.3	6.7×10^5
Different Al/Zr ratio					
2	23	2887	60	51.1	1.6×10^5
2	46	5775	60	12.3	6.8×10^5
2	80	10,043	60	6.1	1.3×10^6

crystallization temperature of various mPE nanocomposites. At lower clay content, the clay exhibits its retardation effect on the crystallization behavior. At higher clay content, however, the clay becomes a nucleation agent that induces fast crystallization kinetics because of its aggregations as in suggested by X-ray diffraction pattern (Fig. 1). In addition, some exfoliated clay also exists at higher content, so that the pure mPE homopolymer always has the fastest rate of crystallization.

The Avrami stretched exponents (n) in crystalline polymers usually have some degree of fluctuation at different crystallization temperatures because of the occurrence of re-crystallization or re-organization processes [14–16]. We applied the Avrami equation to the isothermal crystallization process without considering the lamella-thickness process. The lamella-thickness process is a phenomenon in which the original lamella-thickness increases as a result of polymer

Table 3
Kinetic parameters in the Avrami model and equilibrium melting temperature for metallocence PE nanocomposites from Hoffman–Week plot

Sample	Clay content (wt%)	T_c (°C)	n	k	$t_{1/2}$ (min)	T_m (°C)	T_m^0 (°C)	Stability parameter φ
mPE	0	122	1.74	0.57	1.12	132.0	148.3	0.62
		121	1.62	1.17	0.72	131.9		
		120	1.34	1.67	0.52	131.8		
		119	1.20	2.80	0.31	131.5		
		118	1.17	4.27	0.21	131.4		
		117	1.07	5.13	0.16	131.3		
mPE1	2.4	122	1.15	0.15	3.84	131.2	140.4	0.50
		121	1.16	0.19	3.02	130.7		
		120	1.31	0.37	1.62	130.3		
		119	1.38	0.63	1.06	129.6		
		118	1.44	1.39	0.62	129.3		
		117	1.38	2.70	0.37	129.1		
mPE2	7.3	122	0.95	0.20	3.70	130.7	137.1	0.43
		121	1.19	0.68	1.02	130.3		
		120	1.13	1.18	0.66	130.1		
		119	1.26	2.44	0.37	129.4		
		118	1.13	4.73	0.18	129.2		
mPE3	12.9	122	1.09	0.33	1.95	130.8	135.8	0.35
		121	1.19	0.78	0.90	130.5		
		120	1.16	1.38	0.55	130.3		
		119	1.17	2.73	0.31	129.8		
		118	1.14	4.75	0.18	129.3		

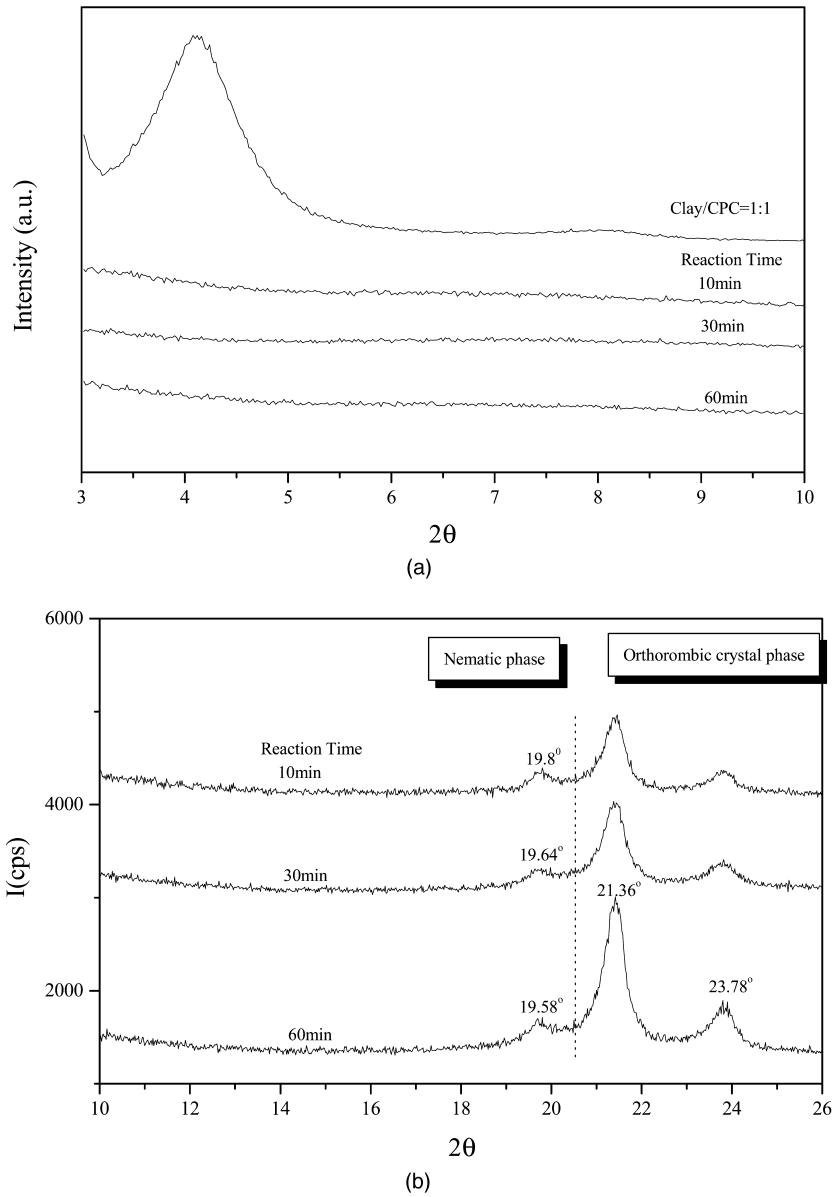

Fig. 4. WAXD pattern of metallocence PE nanocomposites formed by the polymerization pathway in Route 2 at different polymerization times with (a) $2\theta = 3–10^\circ$ and (b) $2\theta = 10–26^\circ$.

chain extension and conformational changes. It has been observed, however, that the lamella-thickness process occurs during annealing of the crystallized PE sample at temperatures between T_g and T_m. At higher clay content, the Avrami stretched exponent (n) is close to constant under different crystallization temperatures. This observation can be explained in terms of the lower degrees of re-crystallization and re-organization occurring in this mPE/clay nanocomposite. Actually, the addition of even more clay can enhance the crystallization rate and stabilize the crystal size by shifting the mechanism from homogenous nucleation in a homopolymer to heterogeneous nucleation in the mPE/clay nanocomposites.

3.5. Determining equilibrium melting temperature and crystal stabilization parameters from Hoffman–Week plots

Equilibrium melting temperatures (T_m^0) of mPE nanocomposite and crystal stability parameters can be obtained from the Hoffman–Week plot [25]:

$$T_m = \varphi T_c + T_m^0(1 - \varphi) \quad (1)$$

where T_c is the isothermal crystallization temperature, T_m is the melting temperature of the isothermal crystallized sample, and φ is the crystal stability parameter. Table 3 lists the fitted stability parameters obtained for pure mPE

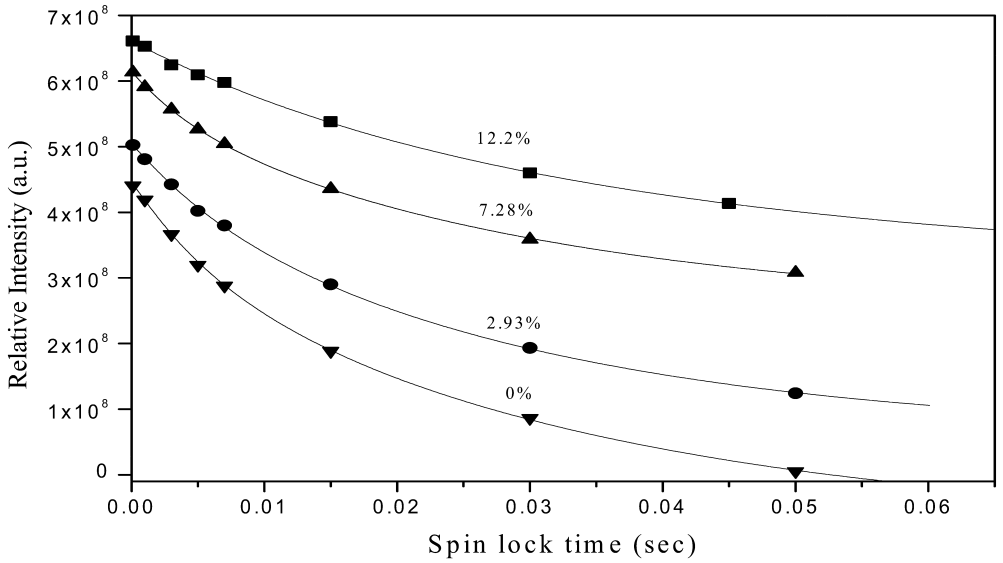

Fig. 5. Solid-state NMR spectroscopic $T_{1\rho}^{H}$ decay curves of mPE nanocomposites formed by polymerization through Route 1.

and various mPE/clay nanocomposites. A reduced stability parameter indicates that the presence of the clay in the nanocomposites increases the crystal stability. By comparing these crystal stability parameters, we conclude that this unstable crystal causes the large fluctuation in the Avrami stretched exponents (n) observed at different crystallization temperatures.

3.6. Kim–Bae theory of equilibrium melting temperature depression

From the modified Flory–Huggins melting temperature depression theory [26], Nishi and Wang [27] have proposed a simple equation to calculate the interaction parameter:

$$\frac{1}{T_m} - \frac{1}{T_m^0} = -\frac{R}{\Delta Hu_2}\left(\frac{V_2}{V_1}\right) \times \left[\ln\left(\frac{w_2^2}{m_1}\right) + \left(\frac{1}{m_1} + \frac{1}{m_2}\right)(1 - w_2) + \chi_{12} w_1^2\right] \quad (2)$$

where T_m is the melting temperature of the isothermal crystallized sample, R is the gas constant, ΔHu_2 is the perfect crystal melting enthalpy per crystallizable polymer, V_i is the molar volume of the components, m_i is the molar mass of the components, w_i is the weight fraction of the components, and χ_{12} is the interaction parameter for

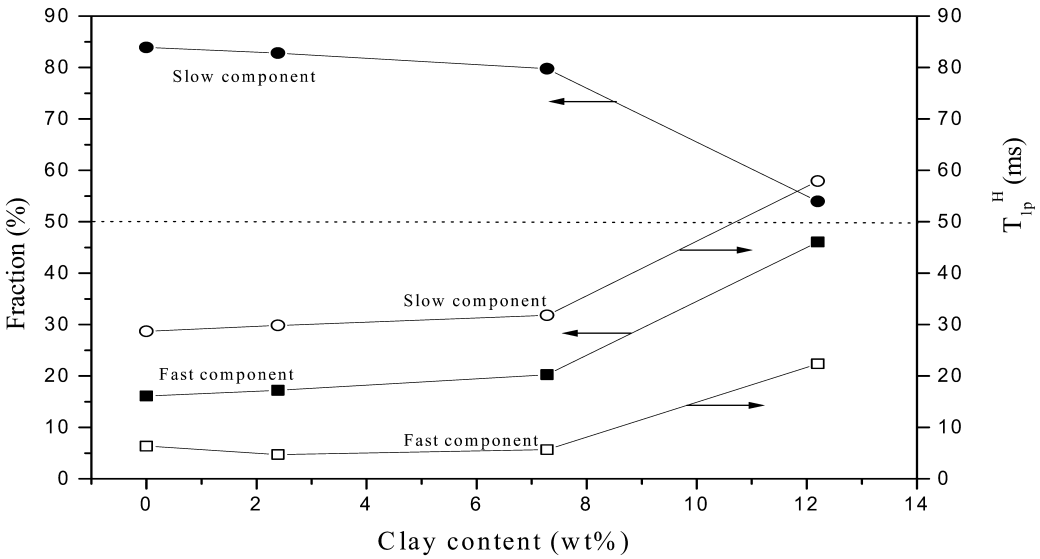

Fig. 6. Effect of clay content on the values of $T_{1\rho}^{H}$ and the relative fraction of its slow and fast components.

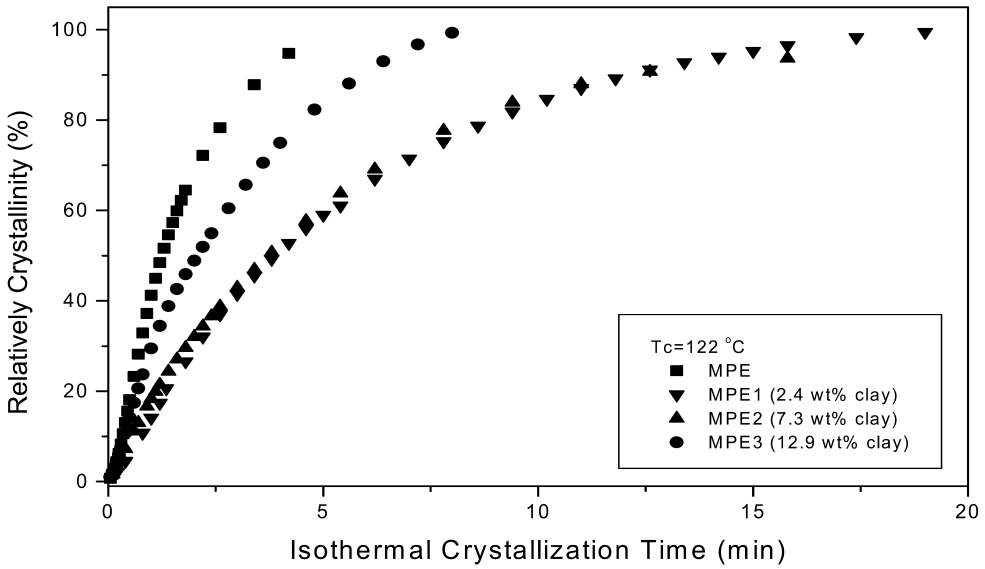

Fig. 7. (a) Crystallization curves of mPE and various mPE nanocomposites at $T_c = 122$ °C.

polymer–polymer and clay–polymer interactions through London dispersion forces.

A new equation for melting point depression, developed by Kim and Bae [17], has been found to fully match the equilibrium melting temperature depression behavior in polymer electrolyte systems. We modified the Kim–Bae equation slightly, as shown by Eq. (3), to fit this mPE/clay nanocomposite system:

$$\frac{1}{T_m} - \frac{1}{T_m^0} = -\frac{R}{\Delta H u_2}\left(\frac{V_2}{V_1}\right) \times\left[A^{DH} + \ln\left(\frac{w_2^2}{m_1}\right) + \left(\frac{1}{m_1} + \frac{1}{m_2}\right)(1 - w_2) + \chi_{12} w_1^2\right] \quad (3)$$

where the A^{DH} as a sum of the strengths of the clay–clay and clay–polymer interactions. Fig. 10 shows the results of fitting our data to both the Nishi–Wang equation and Eq. (3).

In the Kim–Bae theory, the ion–ion interaction in a Debye–Huckel lattice is considered. Increasing the content of an inorganic salt enhances the ion–ion interactions. In our system, the clay has a charged surface so we can consider the system as featuring another type of ion–ion interaction. The strength of this interaction is also expected to be proportional to the Debye–Huckel coefficient (A) and should change with increasing clay content. Because the clay content is less than 15 wt% in these mPE/clay nanocomposites, however, we expect that the value of A^{DH} will be insensitive to the clay content and remain a constant. From Eq. (3), we obtain the

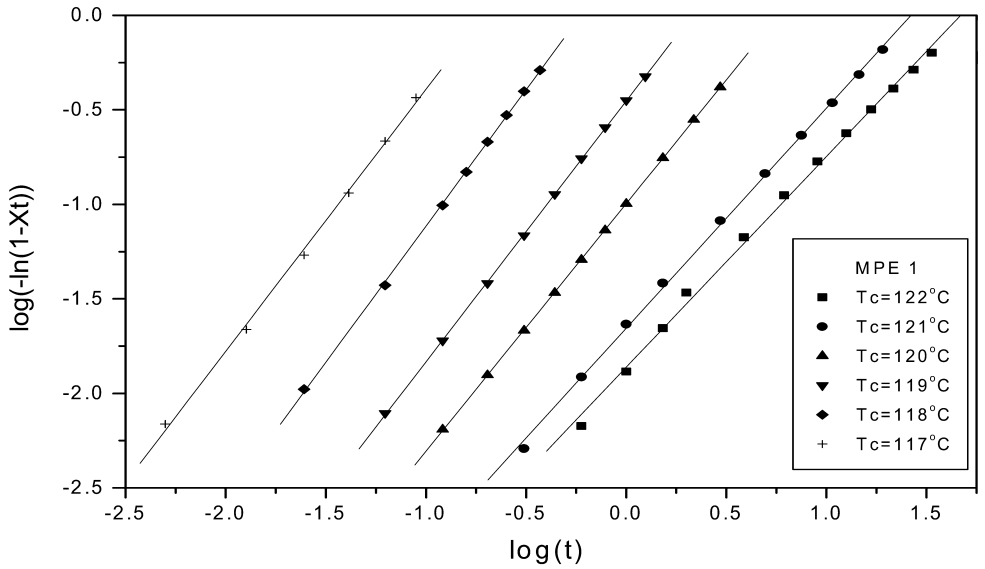

Fig. 8. Results of fitting the Avrami model to the crystallization curves of mPE1 nanocomposites with different isothermal crystallization temperatures.

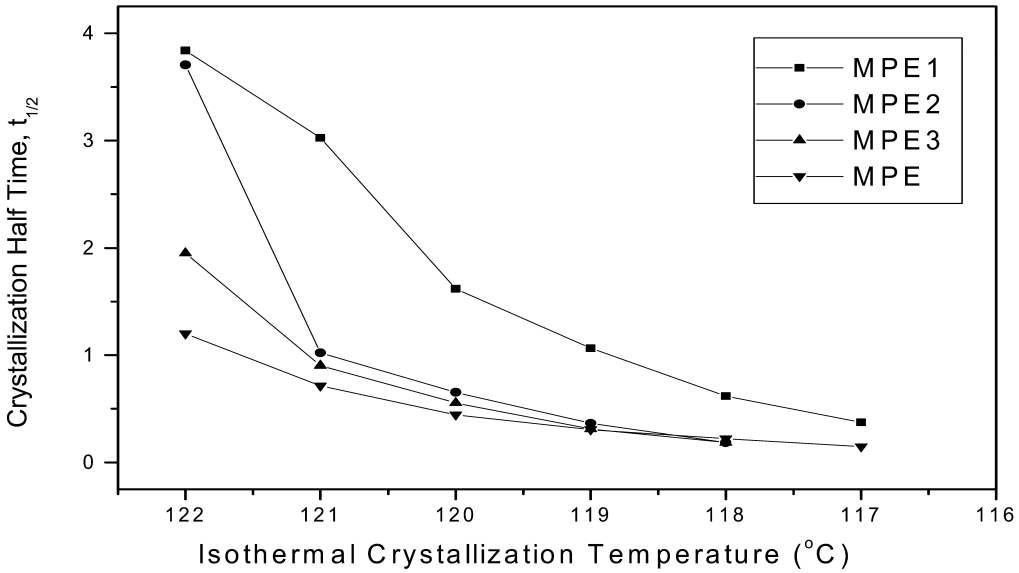

Fig. 9. Plot of half-time of crystallization versus the clay content of mPE nanocomposites.

polymer interaction parameter (χ_{12}) and the value of the strength of the ionic interaction (A^{DH}) between the mPE polymer chains and the exfoliated clay sheets. From the fitted parameter, this polymer interaction parameter (χ_{12}) is equal to -0.205, which is similar to the value found for polymer–polymer interactions in our previous study on hydrogen bonding with a negative polymer interaction parameter [28,29], while the value of strength of the ionic interaction is equal to 3.65. As far as we are aware, this report is the first one in which the effects of ion–ion interactions on the crystallization kinetics have been demonstrated and a modified Kim–Bae equation has been used to explain the behavior of the equilibrium melting temperature depression of this polymer nanocomposite.

4. Conclusions

We have investigated the crystallization behavior, morphology, and molecular motion of mPE/clay nanocomposites by DSC, WAXD, TEM, and solid-state NMR spectroscopy. The polymerization activity and the melting and crystallization enthalpies of polyethylene decrease with increasing clay content. Higher clay content results in faster rates of crystallization, but, even so, it is pure mPE that crystallizes at the fastest rate. In addition, the negative interaction parameter between mPE and exfoliated clay sheets, based on the modification of the Kim–Bae equilibrium melting depression equation, indicates that intermolecular interactions between PE and clay are indeed present. A more homogeneous and finer dispersion of the

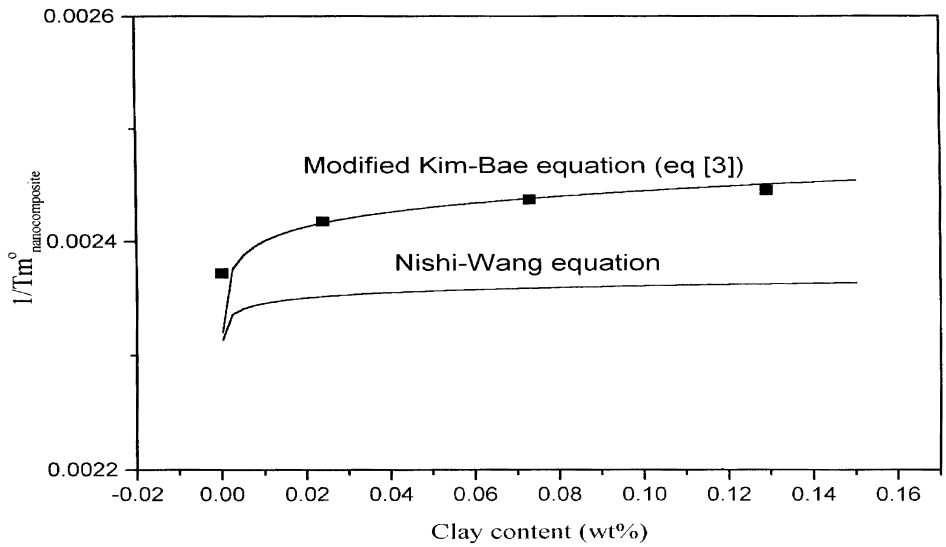

Fig. 10. The behavior of the equilibrium melting point depression of mPE nanocomposites fitted by the Flory–Huggins and Kim–Bae equations.

clay in the polymer matrix can be obtained by using a small quantity of pre-treated clay, as determined by wide-angle X-ray diffraction analysis and transmission electron microscopy. Both of the values of $T_{1\rho}^{H}$ in the solid-state NMR spectra for the fast and slow components show increment with increasing clay content, which indicates that either the mobile phase tends to increase its rigidity or that a nematic phase is possibly formed in the clay-containing system.

References

[1] Kong D, Park CE. Chem Mater 2003;15:419.
[2] Bharadwaj RK. Macromolecules 2001;34:9189.
[3] Biswas M, Ray SS. Adv Polym Sci 2001;155:167.
[4] Giannelis EP, Krishnamoorti R, Manias E. Adv Polym Sci 1999;138:107.
[5] Vaia RA, Giannelis EP. Macromolecules 1997;30:7990.
[6] Benedikt GM, Goodall BL, Marchant NS, Rhodes LF. New J Chem 1994;18:105.
[7] Kaminsky W, Bark A, Arndt M. Macromol Chem Macromol Symp 1991;47:83.
[8] Kaminsky W, Bark A. Polym Int 1992;28:251.
[9] Herfert N, Montag P, Fink G. Makromol Chem 1993;194:3167.
[10] Kaminsky W. Macromol Chem Phys 1996;197:3907.
[11] Chien JCW, He D. J Polym Sci Polym Chem Ed 1991;29:1603.
[12] Carrado K, Xu AL. Chem Mater 1998;10:1440.
[13] Elah AA, Moet A. J Mater Sci 1996;31:3589.
[14] Kamal MR, Chu E. Polym Engng Sci 1983;23:27.
[15] Janimak JJ, Stevens GC. Thermochim Acta 1999;332:125.
[16] Hoffman JD, Miller RL. Polymer 1997;38:3151.
[17] Kim JY, Bae YC. Polymer 1999;40:1979.
[18] Privalko EG, Pedoseuko AV, Privalko VP, Walter R, Friedrich K. J Appl Polym Sci 1999;73:1267.
[19] Privalko EG, Sukhorukov PI, Privalko VP, Walter R, Friedrich K, Balta CJ. J Appl Polym Sci 1999;73:1041.
[20] Clayden NJ. J Polym Sci Polym Phys Ed 1994;32:2321.
[21] Colquhoun IJ, Packer KJ. Br Polym J 1987;19:151.
[22] Packer K, Pope JJ, Yeung RR. J Polym Sci Polym Phys Ed 1984;22:589.
[23] Eckman RR, Henrichs PM, Peacock AJ. Macromolecules 1997;30:2474.
[24] Ginzburg VV, Balazs AC. Macromolecules 1999;32:5681.
[25] Hoffman JD, Weeks JJ. J Chem Phys 1965;42:4301.
[26] Flory PJ. Principles of polymer chemistry. Ithaca, NY: Cornell University Press; 1953.
[27] Nishi TT, Wang T. Macromolecules 1975;8:909.
[28] Kuo SW, Chang FC. Macromolecules 2001;34:4089.
[29] Kuo SW, Chang FC. Macromol Chem Phys 2001;201:3112.